STRONG PULSES NEAR SOURCE FAULTS GENERATED DURING THE 2016 KUMAMOTO, JAPAN, EARTHQUAKES

K. SOMEI[1], K. MIYAKOSHI[1], K. YOSHIDA[1], S, KURAHASHI[2], K. IRIKURA[2]

[1]Geo-Research Institute (GRI), Osaka, Japan

[2]Aichi Institute of Technology (AIT), Toyota, Japan

E-mail contact of main author: somei@geor.or.jp

Abstract. Extremely large ground motions with strong pulses were observed near source faults during two large M_{JMA} 6.5 and M_{JMA} 7.3 events in the 2016 Kumamoto, Japan, earthquakes. In order to investigate the mechanisms of generating strong pulses at near-source station, KMMH16, during both events, we first performed the strong ground motion simulations in a broadband frequency range between 0.2-10 Hz by using the empirical Green's function method. For both the *M*6.5 and *M*7.3 events, strong motion generation area (SMGA) source models were prepared to simulate the ground motions, and they were able to reproduce well the characteristics of observed ground motions in and around the source areas, including the strong pulses at KMMH16. We also carried out the ground motion simulations based on the hypothetical simple source models to discuss the effect of rupture directivity on near-source strong ground motions. The principal findings from the results of these ground motion simulations are follows: 1) During *M*6.5 event, the forward rupture directivity from two SMGAs with strike-slip caused the two distinct strong pulses in fault normal component. 2) During *M*7.3 event, the upward rupture directivity along the fault dip direction from the SMGA with strike-slip including small normal-slip, which is located just beneath KMMH16, caused the strong pulse in both fault parallel and normal components.

Key Words: The 2016 Kumamoto earthquakes, Strong pulse, Strong motion generation area, Empirical Green's function method

1. Introduction

Near-source strong ground motions during large inland crustal earthquakes such as the 1994 Northridge and the 1995 Kobe earthquakes received a great deal of attention from seismological and earthquake engineering communities because of their impact to cause severe earthquake disaster to urbanized area. Following the development of strong motion observation network, many remarkable strong ground motions have been recorded in the last two or three decades, and they urged the studies on the generation mechanisms of near-source strong ground motions. Through incorporating scientific knowledge on near-source ground motion generation into strong ground motion predictions toward future earthquakes, we have been publishing seismic hazard maps and developing the methodology of design basis ground motions for important facilities.

After an M_{JMA} 6.5 inland crustal earthquake (hereafter *M*6.5 event) occurred in Kumamoto prefecture, which is in the central Kyushu Island, southwest Japan, at 21:26 (JST=UT+9) on April 14, 2016, seismic activities have significantly increased in the central Kyushu around Kumamoto prefecture with a maximum M_{JMA} 7.3 event (hereafter *M*7.3 event) occurred at 01:25 on April 16, 2016 (Fig. 1). Based on the observational results from aftershock

distributions (e.g., Kato et al., 2016[5], Uchide et al., 2016[6]), field surveys (e.g., Sugito et al., 2016[7], Shirahama et al., 2016[8]) and ALOS-2/PALSAR-2 data (e.g., Ozawa et al., 2016[9], Fujiwara et al., 2016[10]), these earthquakes (hereafter the 2016 Kumamoto earthquakes) mainly occurred along the Futagawa fault zone and the northern part of the Hinagu fault zone, both is referred to collectively as the Futagawa-Hinagu fault system, which is one of the major active fault systems with right-lateral strike slip fault type on Kyushu Island.

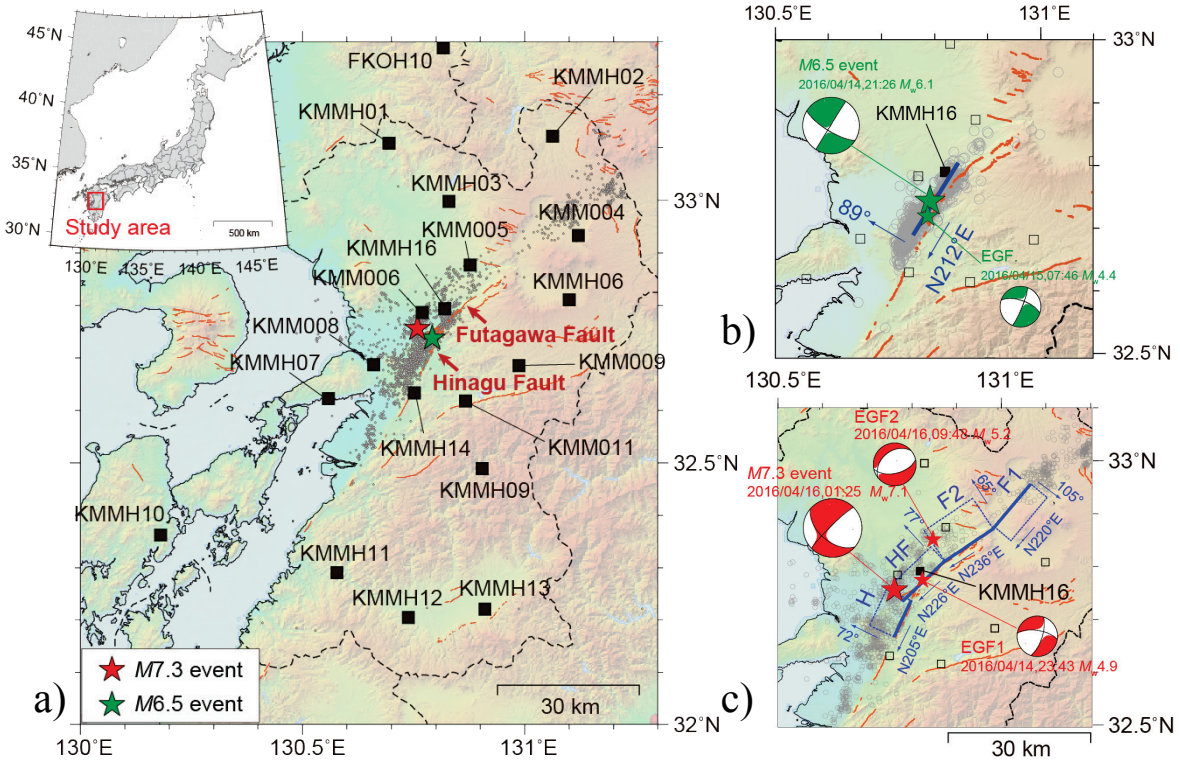

FIG. 1. a) Map showing the study area. Red and Green stars denote epicenters of M7.3 and M6.5 events, respectively. Black squares indicate strong motion stations used in this study. Small gray circles correspond to the epicenters of events within 6 days after the M6.5 event. Orange lines represent surface traces of active faults compiled by Nakata and Imaizumi (2002)[1]. b) Epicenters of M6.5 and EGF event with their moment tensor solutions determined by broadband seismograph network F-net of NIED (Fukuyama et al., 1998[2]). The blue rectangle (line) represents surface projection of assumed source fault plane of M6.5 event based on the source inversion model by Asano and Iwata (2016)[3]. c) Epicenters of M7.3 and EGF events with their moment tensor solutions determined by F-net. Blue rectangles (lines) represent surface projections of assumed source fault planes of M7.3 event based on the source inversion model by Yoshida et al. (2017)[4].

The 2016 Kumamoto earthquakes caused the severe damage through the strong ground-shaking, surface ruptures, and subsequent landslides with killing at least 200 people including disaster-related death, injuring about 2800 others, and completely collapsing more than 8500 buildings in and around the Kumamoto prefecture, centering on Mashiki town in particular, which is typical residences in Japan (FDMA, 2018[11]). Two dense nationwide digital strong motion seismograph networks, K-NET and KiK-net, both installed and operated by the National Research Institute for Earth Science and Disaster Resilience, Japan (NIED) (Aoi et al., 2011[12]), recorded the ground acceleration time histories with near-source strong ground motions during the 2016 Kumamoto earthquakes (Fig. 2). Figure 2 shows the large ground motions locally observed at stations in more than 70 km northeast from the epicenter during *M*7.3 event, which were attributed to the local induced earthquake in Oita region (Suzuki et al., 2017[13]). For both of the *M*6.5 and *M*7.3 events, extremely large ground motions with

maximum peak ground accelerations (PGAs) over 1000 cm/s^2 were observed at KMMH16 station, in Mashiki town, which is the closest station to the source fault within K-NET and KiK-net networks: KMMH16 is located about 6 and 7 km away from epicenters of *M*6.5 and *M*7.3 events, respectively. Figure 3 shows observed velocity waveforms in fault parallel (FP) and normal (FN) components at KMMH16 during *M*6.5 and *M*7.3 events. For *M*6.5 event, two velocity pulses were clearly seen in FN component, whereas for *M*7.3 event, a large velocity pulse was observed FP component as well as FN component.

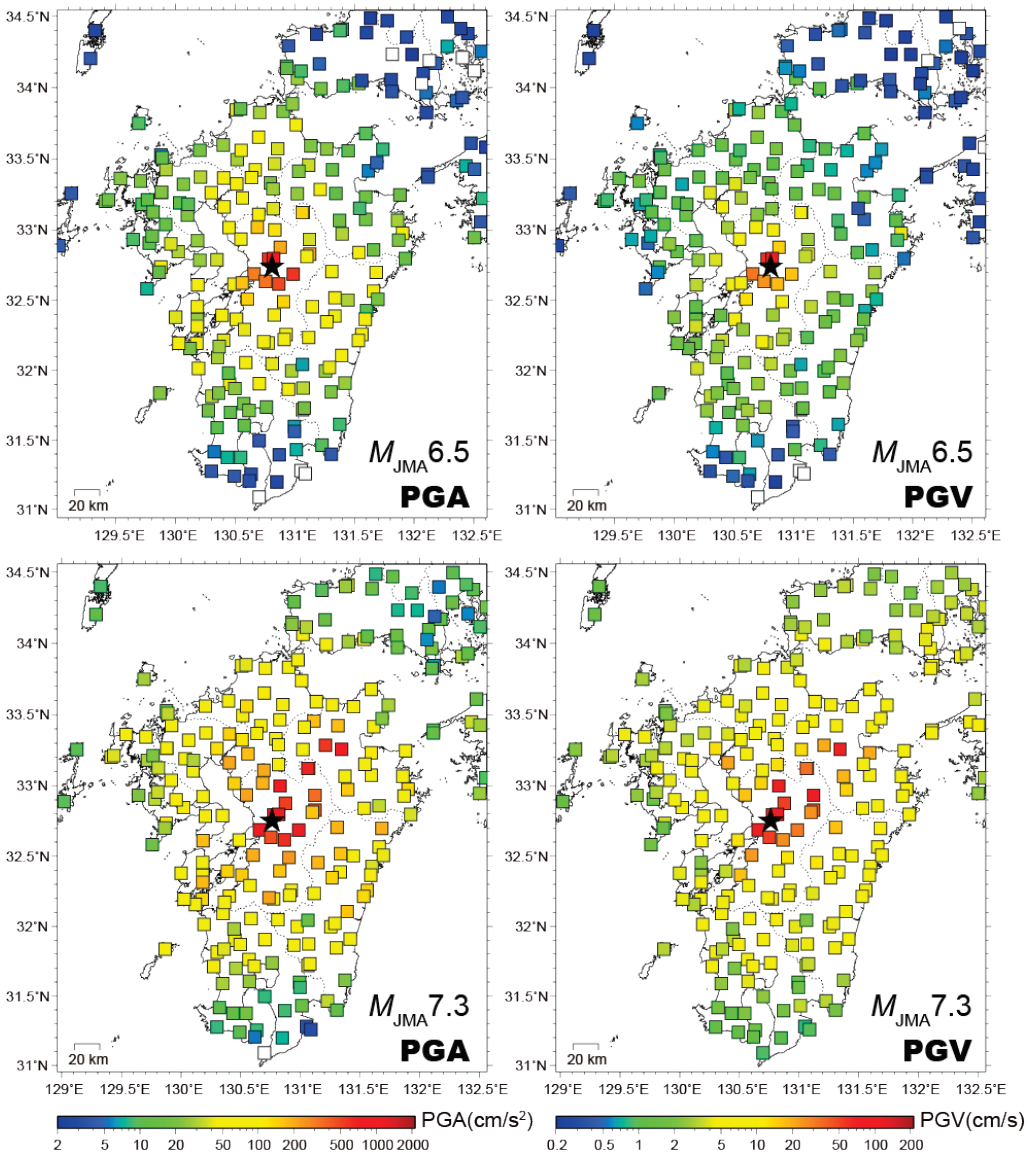

FIG. 2. a) Spatial distributions of PGA (left) and PGV (right) for K-NET and KiK-net stations. Upper and lower panels indicate the M6.5 and M7.3 events, respectively. Stars denote the epicenters for each event.

For understanding the physical mechanisms of the ground motion generation processes and/or surface ruptures during the 2016 Kumamoto earthquakes, mainly for *M*7.3 event, kinematic heterogeneous slip histories on the source faults were estimated in space and in time by inversion analyses of teleseismic data (e.g., Yagi et al., 2016[14]), strong motion data (e.g., Asano and Iwata, 2016[3], Kubo et al., 2016[15], Yoshida et al., 2016[4]), both teleseimic and strong motion data (e.g., Hao et al., 2017[16]), and combined datasets from teleseismic, strong

motion, and geodetic data (e.g., Kobayashi et al., 2017[17]). However, those studies used the ground motion data in the frequency range below 1 Hz. In order to accounts for observed strong ground motions in a broadband frequency range, including higher than 1 Hz, which are indispensable to seismic damage on buildings and civil structures. Irikura et al., (2017)[18] constructed the source model consisting of Strong Motion Generation Areas (SMGAs: Miyake et al., 2003[19]), which are defined as high slip velocity or large stress drop areas on the source fault, to reproduce the strong ground motions in 0.2-10 Hz during *M*7.3 event. They used the empirical Green's function (EGF) method (e.g., Irikura, 1986[20]), which use the records of small events occurring close to the target event as empirical Green's function, to simulate the ground motions in such a broadband frequency range, and indicated the applicability of scaling relationship of inland crustal earthquakes in Japan to explain the ground motions of *M*7.3 event in Kumamoto earthquakes.

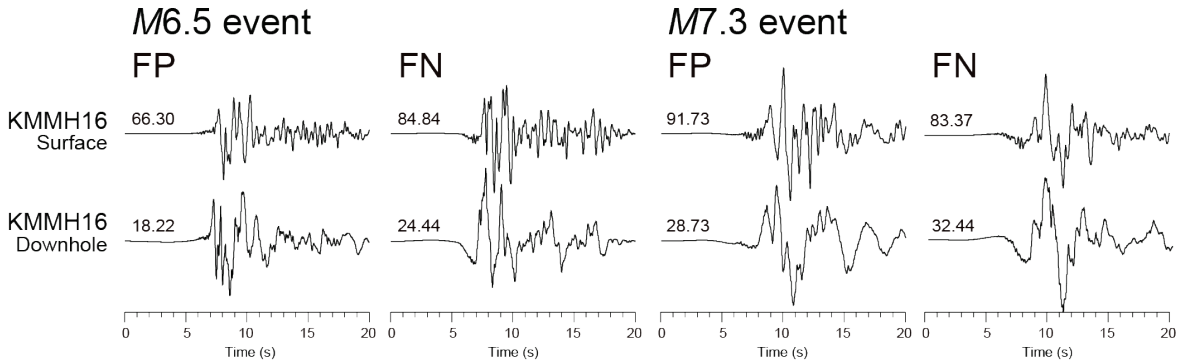

FIG. 3. Velocity waveforms observed in 0.2-10 Hz at KMMH16 during the M6.5(Left) and M7.3(Right) events. FP and FN mean fault parallel and normal components according to the fault strike angle of N212°E for M6.5 event and N226°E for M7.3 event, respectively. Upper and lower panels represent the waveforms recorded at surface and downhole sensors, respectively. Depth of downhole sensor at KMMH16 is 252 m. The maximum amplitude of the waveforms is shown above each trace in cm/s

One of the essential questions raised from the 2016 Kumamoto earthquakes is how to generate the near-source strong ground motions with strong velocity pulses at KMMH16 during both *M*6.5 and *M*7.3 events. Toward addressing this question, reliable source models to explain observed broadband ground motions in and around the source areas are necessary. This paper focused on the SMGA source models for both *M*6.5 and *M*7.3 events, which gave rise to extreme ground motion with strong velocity pulses near source faults. For *M*6.5 event, we originally estimated a two-SMGA model by broadband ground motion simulations at K-NET and KiK-net stations using EGF method. For *M*7.3 event, a three-SMGA model constructed by Irikura et al., (2017)[18] was used for simulating the ground motions. In the following sections, we first describe the source modeling mainly for *M*6.5 event, and then we discuss about strong ground motion generation processes at KMMH16 during both *M*6.5 and *M*7.3 events.

2. Data

Figure 1 shows the spatial distribution of the strong motion stations of K-NET and KiK-net stations used in this study. The location of each station is listed in Table 1. For *M*6.5 event, 6 K-NET and 11 KiK-net stations are used. For *M*7.3 event, 4 K-NET and 13 KiK-net stations are used. The downhole records of KiK-net stations installed in the basement rock are mostly

used to avoid the soil nonlinearity effects of superficial layers during strong ground motions. The original records are the three components of acceleration time histories sampled at 100 Hz for K-NET and KiK-net stations. All the observed acceleration waveform data are band-pass filtered between 0.2 and 10 Hz using a Chebyshev Type I recursive filter.

TABLE 1: STATION LIST USED IN THIS STUDY.

[*1] INDICATION USED FOR EACH EVENT.

Station code	Latitude (°N: WGS)	Longitude (°E: WGS)	Network	Location	*M*6.5 event[*1]	*M*7.3 event[*1]
KMM004	32.9320	131.1214	K-NET	Ichinomiya	○	
KMM005	32.8761	130.8774	K-NET	Ohdu	○	○
KMM006	32.7934	130.7772	K-NET	Kumamoto	○	○
KMM008	32.6878	130.6582	K-NET	Uto	○	
KMM009	32.8267	131.1226	K-NET	Yabe	○	○
KMM011	32.6858	130.9856	K-NET	Tomochi	○	○
KMMH01	33.1089	130.6949	KiK-net	Kahoku	○	○
KMMH02	33.1220	131.0629	KiK-net	Oguni	○	○
KMMH03	32.9984	130.8301	KiK-net	Kikuchi	○	○
KMMH06	32.8114	131.1010	KiK-net	Hakusui	○	○
KMMH07	32.6234	130.5584	KiK-net	Mizumi	○	
KMMH09	32.4901	130.9046	KiK-net	Izumi	○	○
KMMH10	32.3151	130.1811	KiK-net	Shinwa	○	○
KMMH11	32.2918	130.5777	KiK-net	Ashikita	○	○
KMMH12	32.2054	130.7371	KiK-net	Hitoyoshi		○
KMMH13	32.2209	130.9096	KiK-net	Ue		○
KMMH14	32.6345	130.7521	KiK-net	Toyono	○	○
KMMH16	32.7967	130.8199	KiK-net	Mashiki	○	○
FKOH07	33.3678	130.6354	KiK-net	Tachiarai		○
FKOH10	33.2891	130.8170	KiK-net	Ukiha	○	○

3. SMGA source models through broadband strong motion simulations

As mentioned above, we used the EGF method (e.g., Irikura, 1986[20]) to simulate the ground motions over a wide frequency range. The EGF method is a technique used to synthesize seismic records by summing up the observed records of small earthquakes as empirical Green's functions. In general, calculating a Green's function from source to station, which explains in higher frequency range, is difficult, because we do not know a detailed 3D underground structure. From that point of view, a clear advantage in EGF method is what we directly know the Green's function by using the observed records of small earthquake. Hereafter we call the small earthquake as 'EGF event'.

3.1. SMGA model for *M*6.5 event

For modeling the SMGA of the *M*6.5 event, we used records of an M_w 4.4 aftershock whose source parameters are listed together with those of *M*6.5 event in Table 2. The EGF event had

a similar focal mechanism to the *M*6.5 event and was located at the southwest near the epicenter of *M*6.5 event (Fig. 1b). From the observed waveforms at KMMH16 during the *M*6.5 event shown in Fig. 3, we could see that S-wave portion consists mainly of two wave packets. These two S-wave packets were clearly observed in the records at strong motion stations located surrounding the source area. Also, heterogeneous slip model inverted from strong motion records by Asano and Iwata (2016)[3] showed two large slip areas on the fault: One was found near the hypocenter. Another was identified on shallow and northeast side from the hypocenter, which is located just beneath the Mashiki town. Based on these observations, we assumed two squared SMGAs on the source fault using the same hypocenter location and fault geometry as those used in Asano and Iwata (2016)[3].

TABLE 2: SOURCE PARAMTERS OF *M*6.5 EVENT AND THE EGF EVENT.

	*M*6.5 event	EGF event
Origin time (JST=UT+9) *1	2016/04/14 21:26	2016/04/15 07:46
Epicentral Latitude*1	32.7417°N	32.7300°N
Epicentral Longitude*1	130.8087°E	130.7970°E
Hypocentral depth*1	11.39 km	10.52 km
Focal mechanism (Strike, Dip, Rake) *2	(212, 89, -164)	(22, 82, -155)
Seismic moment (M_w) *2	1.74×10^{18} Nm (6.1)	4.19×10^{15} Nm (4.4)

*1 Japan Meteorological Agency (JMA)
*2 F-net

Under the assumption of the ω^{-2} source spectral model, two scaling parameters N and C are necessary in EGF method by Irikura (1986)[20]: N and C are the ratios of the source dimensions and the stress drops between the target and EGF events, respectively. In this paper, we generally followed the procedures of Miyake et al. (2003)[19] to determine these parameters by fitting the observed source spectral ratio between the target and EGF events to the theoretical source spectral ratio following the ω^{-2} source spectral model. The moment ratio was given by the seismic moments obtained from the moment tensor solutions by F-net. The corner frequencies for the target and EGF events were estimated by the grid search algorithm. Firstly, the observed source spectral ratio for each station was calculated from the Fourier amplitude spectra of direct S-wave portion with correcting the propagation path effects for geometrical spreading for the body waves and an attenuation factor: The frequency-dependent quality factor $Q_S = 62f^{0.87}$ obtained by Satoh (2016)[21] in this region was used to correct the attenuation factor. The S-wave velocity was assumed to be 3.4 km/s based on the Japan Seismic Hazard Information Station (J-SHIS) for deep sedimentary layers model V2 (hereafter 'J-SHIS model'), which is a nation-wide 3D velocity structure model from the seismic bedrock to the engineering bedrock (Fujiwara et al., 2009[22], 2012[23]). Figure 4 shows the observed source spectral ratio, which is obtained from the strong motion records at F-net stations, with the theoretical ω^{-2} source spectral ratio model estimated by the grid search. Based on the straightforward values from the estimated corner frequencies and seismic moments of F-net considering with the partition coefficient in the case of multi-SMGA model (Miyake et al., 2003[19]), N and C for each SMGA were commonly determined as 4 and 1.50, respectively, by waveform fitting in observations and simulations during the *M*6.5 event.

We performed ground motion simulations in the broadband frequency range from 0.2 to 10 Hz, depending on the signal to noise ratio of the records for EGF event, to construct the

SMGA model for the *M*6.5 event. Six parameters for SMGAs representing the size (length and width), position (rupture starting point), rise time, rupture velocity, and stress drop, were estimated by minimizing the residuals of both acceleration envelope and displacement waveform fittings between observations and simulations for 20 sec including S-wave portions in three components. The fitting was done by forward modeling with trial and error method. Following this approach, we estimated SMGAs for the *M*6.5 event as shown in Fig. 5. The estimated parameters of SMGAs are listed in Table 3. The simulated waveforms radiated from two SMGAs, which located close to the large slip areas of kinematic source model by Asano and Iwata (2016)[3], could reproduce the observed waveforms in and around the source area (Fig. 6). The estimated stress drop of both of two SMGAs was 15.3 MPa, which is comparable to the averaged value of past large inland crustal earthquakes in Japan.

TABLE 3: ESTIMATED PARAMETERS OF SMGAS FOR THE *M*6.5 EVENT.

		SMGA1	SMGA2
Length	L (km)	4.0	4.0
Width	W (km)	4.0	4.0
Area	S (km^2)	16.0	16.0
Rise time	τ (s)	0.24	0.40
Seismic moment	M_0 (Nm)	4.02×10^{17}	4.02×10^{17}
Stress drop	$\Delta\sigma$ (MPa)	15.3	15.3
Rupture velocity	V_r (km/s)	2.8	2.8

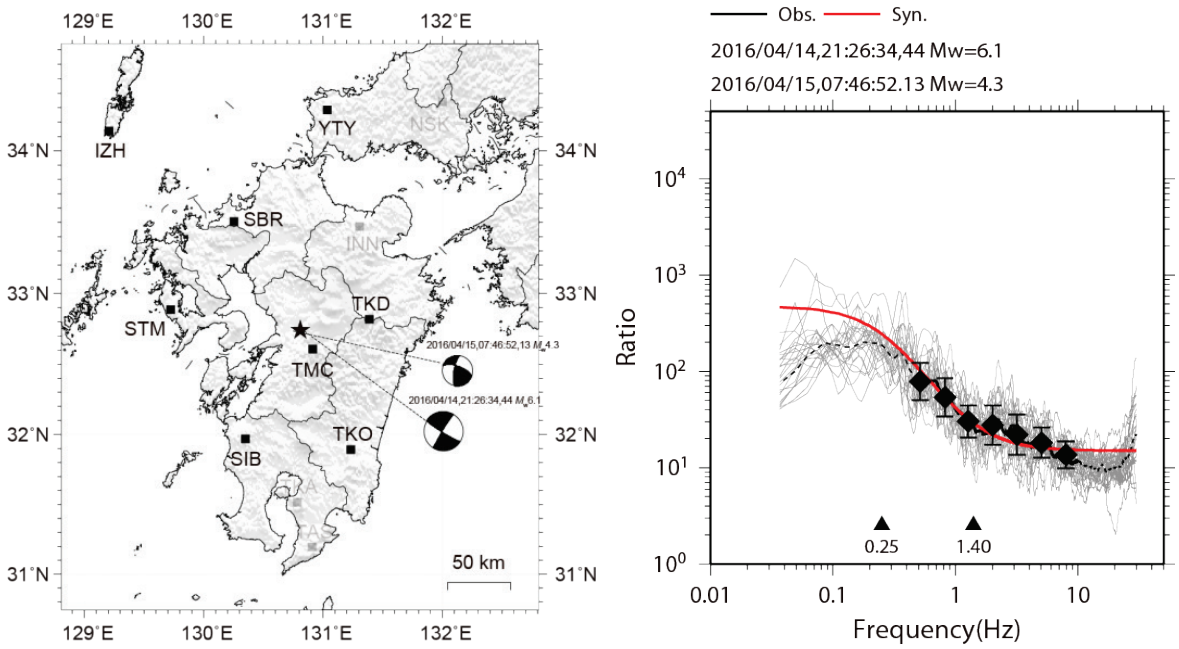

FIG. 4. Left) Spatial distributions of F-net stations used in spectral ratio analysis. Stars represent the epicenters of M6.5 and EGF events with their moment tensor solutions from F-net. Right) Observed source spectral ratios for each station (thin gray lines), the average observed source spectral ratios among stations (thick black line), and theoretical source spectral ratio (red line) fitted to the observation. Solid triangles indicate the corner frequencies for M6.5 and EGF events, respectively.

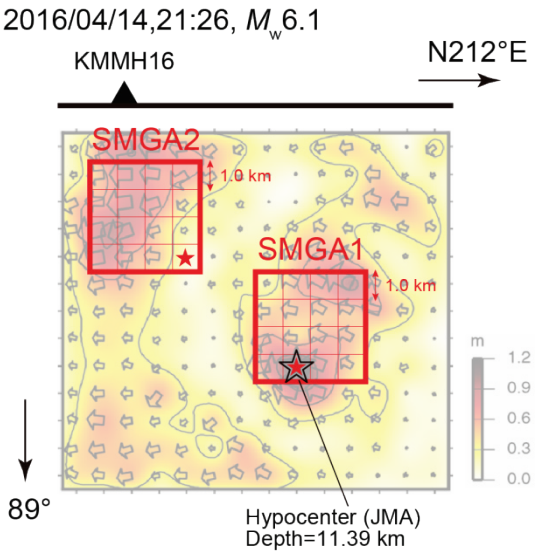

FIG. 5. SMGA source model and slip distribution deduced by Asano and Iwata (2016) [3] *for the M6.5 event. Red rectangles are the estimated SMGA with red stars indicating the rupture starting point. Black open star is the hypocenter of M6.5 event.*

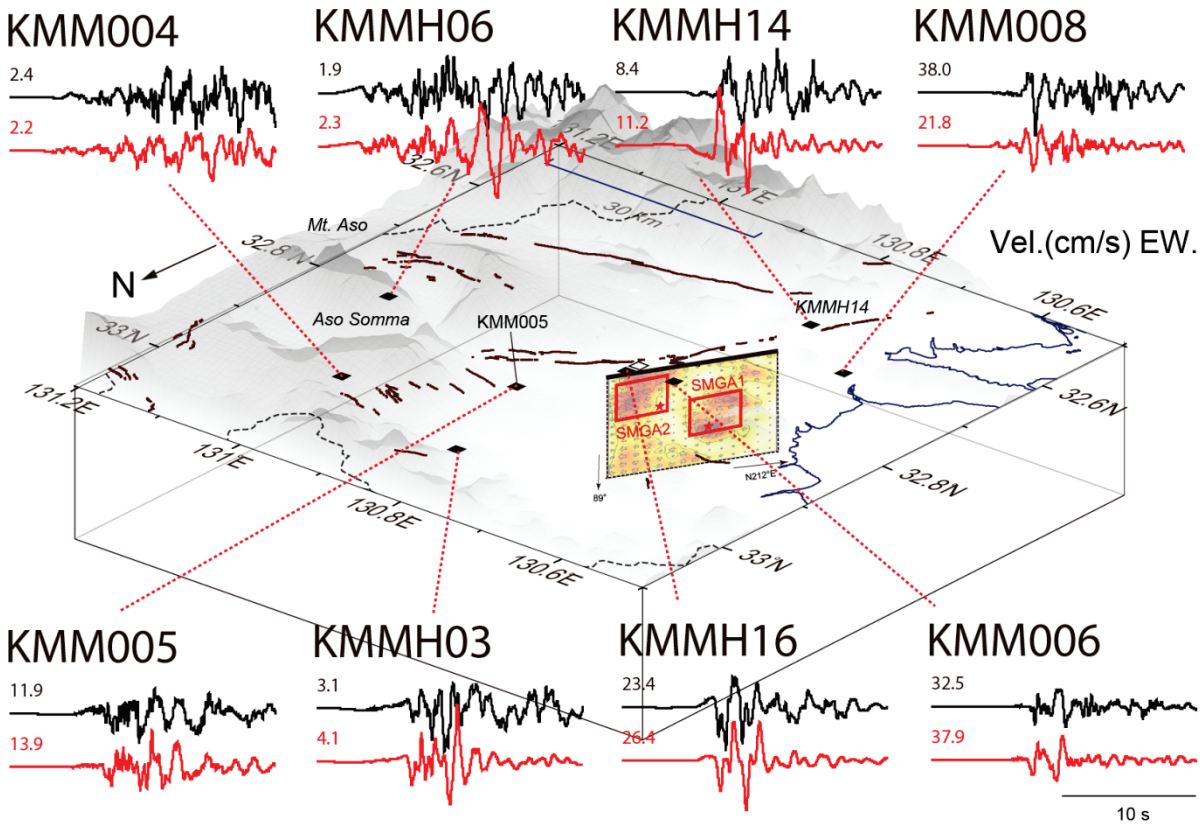

FIG. 6. Birds eye view of source model for M6.5 event. Red rectangles on the slip model by Asano and Iwata (2016)[3] *represent the SMGAs. Rupture starting point of each SMGA is indicated by red star. Black squares show the strong motion stations with observed (black) and simulation (red) velocity waveforms in EW component (0.2-10 Hz). The maximum amplitude of the waveforms is shown above each trace in cm/s.*

3.2. SMGA model for *M*7.3 event

Irikura et al., (2017)[18] has constructed SMGA source model for the *M*7.3 event by broadband strong ground motion simulations in 0.2-10 Hz using the EGF method. Their three-SMGA model was estimated on the multi-segment fault model setting along the Futagawa-Hinagu fault system by Yoshida et al. (2016)[4], whose fault geometries are shown in Fig. 1c. Figure 1c also shows the epicenters of the *M*7.3 event and two EGF events with their moment tensor solutions of F-net. The source parameters of these events are listed in Table 4. Figure 7 shows the SMGA model, whose parameters are listed in Table 5, and the spatial distribution of peak moment rate from kinematic heterogeneous source model by Yoshida et al. (2016)[4]. The three squared SMGAs were identified near the large peak moment rate areas. The rupture inside SMGA1 propagated in southwest direction from the hypocenter of the *M*7.3 event. SMGA2 was located just beneath the KMMH16 and its rupture mainly propagated toward the up-dip direction. The rupture of SMGA3 propagated in northeast direction. The stress drops of three SMGAs were 13.4 and 13.6 MPa, which is comparable to the averaged value of past large inland crustal earthquakes in Japan.

In this paper, ground motion simulations for the *M*7.3 event was carried out based on that three-SMGA model. Figure 8 shows the comparison of velocity waveforms between observations and simulations in EW component at strong motion stations surrounding the source area. Although simulations satisfactorily explained the main characteristics of the observed waveforms for most of stations, some discrepancy could be seen in the northeast side from the source fault. There are still scopes to improve the parameters of the SMGA located in the Futagawa fault segment, which is effective to the ground motions in the northeast side of source fault such as KMMH06.

TABLE 4: SOURCE PARAMTERS OF *M*7.3 EVENT AND THE EGF EVENT.

	*M*7.3 event	EGF1 event	EGF2 event
Origin time (JST=UT+9) [*1]	2016/04/16 01:25	2016/04/14 23:43	2016/04/16 09:48
Epicentral Latitude[*1]	32.7545°N	32.7670°N	32.8470°N
Epicentral Longitude[*1]	130.7630°E	130.8273°E	130.8350°E
Hypocentral depth[*1]	12.45 km	14.20 km	15.91 km
Focal mechanism (Strike, Dip, Rake) [*2]	(226, 84, -142)	(279, 67, -22)	(230, 38, -112)
Seismic moment (M_w) [*2]	4.42×10^{19} Nm (7.1)	2.71×10^{16} Nm (4.9)	6.27×10^{16} Nm (5.2)

[*1] Japan Meteorological Agency (JMA)
[*2] F-net

TABLE 5: ESTIMATED PARAMETERS OF SMGAS FOR THE *M*7.3 EVENT.

		SMGA1	SMGA2	SMGA3
Length	L (km)	7.2	7.2	10.0
Width	W (km)	7.2	7.2	10.0
Area	S (km^2)	51.8	51.8	100.0
Rise time	τ (s)	0.6	0.6	0.6
Seismic moment	M_0 (Nm)	2.08×10^{18}	2.08×10^{18}	5.49×10^{18}
Stress drop	$\Delta\sigma$ (MPa)	13.6	13.6	13.4
Rupture velocity	V_r (km/s)	2.8	2.8	2.8
EGF event	-	EGF1	EGF1	EGF2

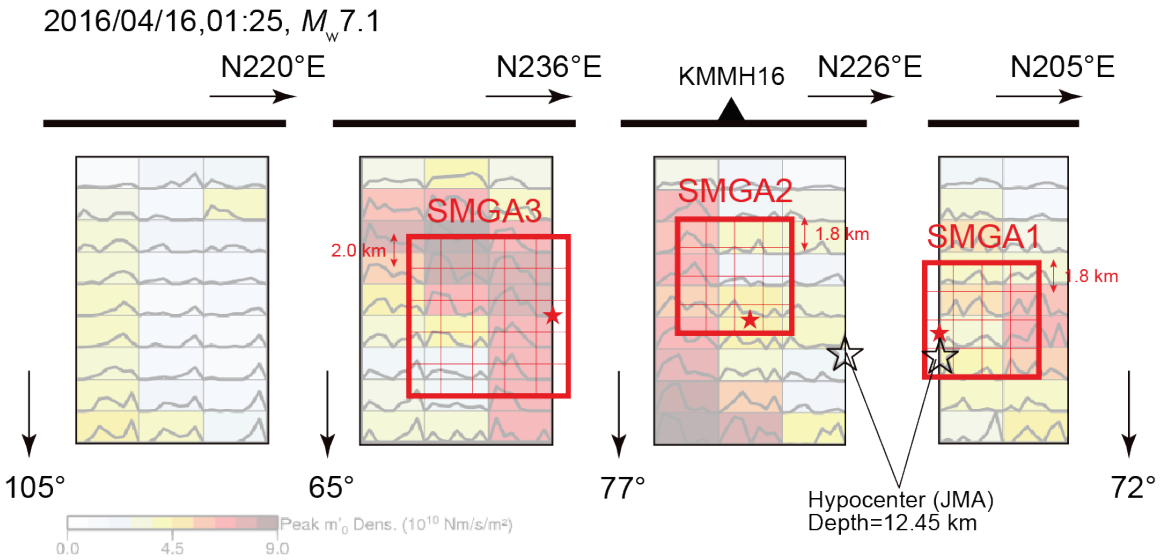

FIG. 7. Three-SMGA source model by Irikura et al. (2017)[18] and the spatial distribution of peak moment rate on the source fault from kinematic inversion model by Yoshida et al. (2017)[4] for the M7.3 event. Red rectangles are the estimated SMGA with red stars indicating the rupture starting point. Black open star is the hypocenter of M7.3 event.

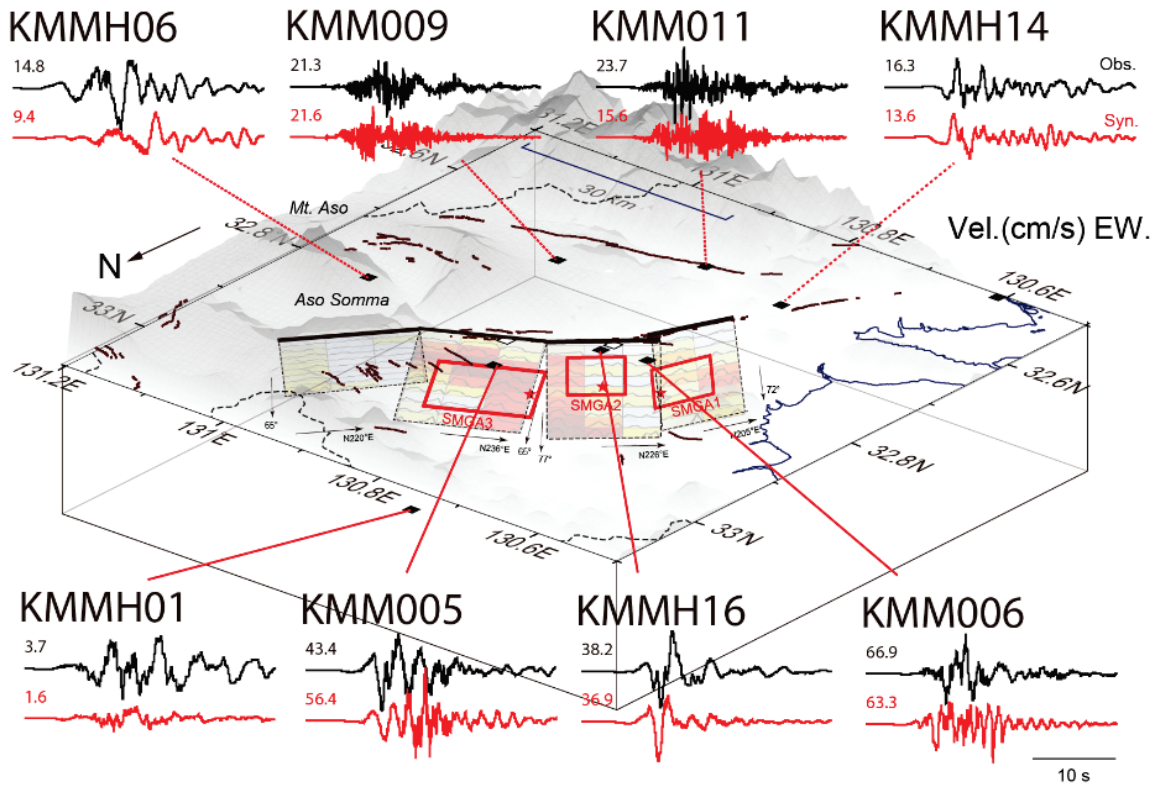

FIG. 8. Birds eye view of source model for M7.3 event. Red rectangles on the kinematic inversion model by Yoshida et al. (2017)[4] represent the SMGAs by Irikura et al. (2017)[18]. Rupture starting point of each SMGA is indicated by red star. Black squares show the strong motion stations with observed (black) and simulation (red) velocity waveforms in EW component (0.2-10 Hz). The maximum amplitude of the waveforms is shown above each trace in cm/s.

4. Discussion

In order to reveal the mechanisms of generating strong pulses at near-source station KMMH16 during both *M*6.5 and *M*7.3 events, we first discuss about the observed and simulated velocity waveforms at KMMH16 during both events, focusing on the contributions of each SMGA and the rupture directions to strong pulses. We also demonstrate a set of simple ground motion simulations to discuss the importance of rupture direction inside the SMGA in strong pulse near source fault.

4.1. Observed and simulated waveforms at KMMH16

Figure 9 shows the comparisons between the observed and simulated velocity waveforms in 0.2-10 Hz at KMMH16 during the *M*6.5 and *M*7.3 events with the contributions of each SMGA to simulated waveforms. For *M*6.5 event, two strong pulses in FN component observed at KMMH16 were well explained by the simulations contributed from each of SMGAs. These pulses in FN components could be generated by the forward rupture directivity effect of SMGAs with strike-slip on vertical fault: The rupture in SMGA mainly propagated in northeast direction along the fault strike, which propagated toward KMMH16 from the hypocenter. This kind of 'forward rupture directivity effect' to generate the strong pulse in FN component has also observed during the 1995 Kobe earthquake (e.g., Kamae and Irikura, 1998[24]) in Japan.

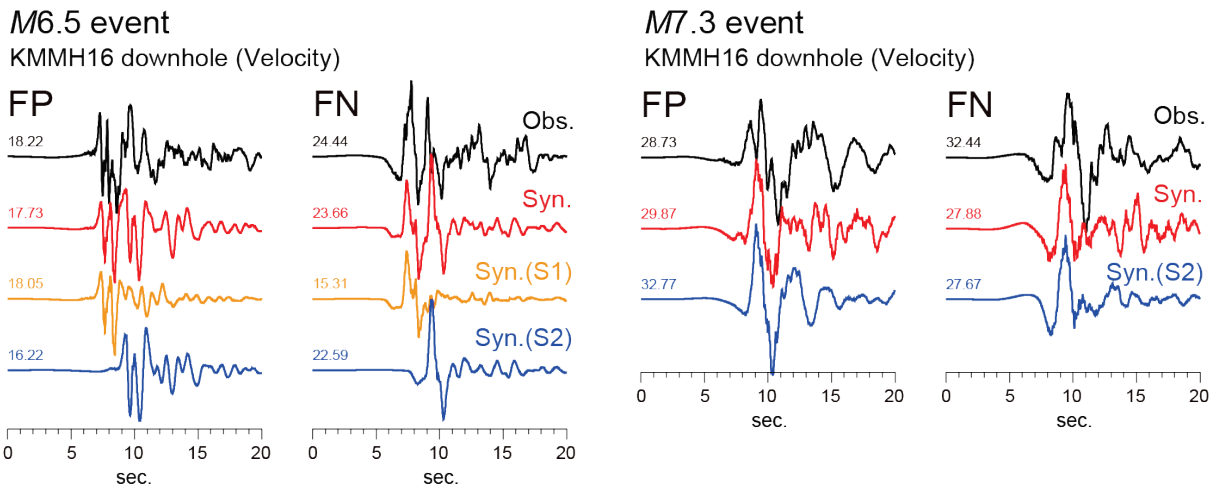

FIG. 9. Comparisons between the observed (black) and simulated (red) velocity waveforms in FP and FN components at KMMH16 during the M6.5 event (left panel) and M7.3 event (right panel). Orange and blue lines represent the simulations from SMGA1 and 2, respectively. The maximum amplitude of the waveforms is shown above each trace in cm/s.

On the other hand, the observed near-source ground motions with strong pulses in velocity waveforms were observed in both FP and FN components at KMMH16 during *M*7.3 events. These strong pulses were successfully reproduced by the simulated waveforms mainly generated from SMGA2 (Fig. 9). The rupture inside SMGA2, located just beneath the KMMH16 site, started from the bottom of SMGA2 and propagated up-dip direction toward KMMH16. Because of this rupture directivity (hereafter we call 'upward directivity') effect, which is caused by the constructive interference of the radiated waves in FP component from SMGA2 with strike-slip, a strong pulse was generated at KMMH16.

4.2. Scenario ground motion simulations using hypothetical source models

For understanding the forward and upward rupture directivity effects on ground motions in FN and FP components at near-source sites, we calculated synthetic ground motions taking into account the scenarios on three hypothetical simple source models with the same seismic moment, size, position, and fault geometry, but with the different rupture starting point and rake angle (Fig. 10). The source parameters assumed in those source models are summarized in Table 6. The ground motion simulations are performed by using the discrete wavenumber method (Bouchon, 1981[25]) with the reflection and transmission matrix method (Kennett and Kerry, 1979[26]). The underground structure model used in this simulation was assumed to be a simple layered half-space medium, which described as P-wave velocity of 6.0 km/s, S-wave velocity of 3.4 km/s, density of 2.75 kg/m3, and Q value of 300. The calculation points were set on ground surface distributed the area of 20 × 20 km spacing with every 1 km for each direction, including the source fault.

TABLE 6: SOURCE VARIABLES USED IN STRONG MOTION SIMULATION.

		Case 1	Case 2	Case 3
Length	L (km)	7.0	7.0	7.0
Width	W (km)	7.0	7.0	7.0
Area	S (km^2)	49.0	49.0	49.0
Seismic moment	M_0 (Nm)	2.0×10^{18}	2.0×10^{18}	2.0×10^{18}
Strike	*Str. (deg.)*	0	0	0
Dip	*Dip (deg.)*	77	77	77
Rake	*Rak. (deg.)*	0	0	-20
Rise time	τ (s)	1.2	1.2	1.2
Average slip	D (m)	1.3	1.3	1.3
Rupture velocity	V_r (km/s)	2.8	2.8	2.8
Rupture starting point	-	North-Bottom	Center-Bottom	Center-Bottom

The spatial distributions of peak horizontal ground velocity (PGV) bandpass-filtered between 0.1 and 3 Hz at the ground surface obtained in the ground motion simulations are shown in Fig. 11. Figure 12 also shows the synthetic velocity waveforms in 0.1-3.0 Hz at the sites located along the fault strike. In Case 1, unilateral rupture propagation exhibited the stronger FN motions relative to FP motions along the fault trace, in particular, the strongest motion was appeared in FN component around the terminal point of the fault rupture, due to the forward rupture directivity effect from the strike-slip fault. This result could represent the strong pulse in FN component observed at KMMH16, located the edge of the fault trace, during M6.5 event. In Case 2, the ground motion near the center of the fault trace was stronger in FP component than that in FN component. This is caused by the upward directivity effect from the strike-slip fault. However, the strong pulse at KMMH16 during M7.3 event was also observed in FN component as well as in FP component. To explain this observation in terms of the source model, we tried to simulation in Case 3, which has same source parameters with Case 2 except the rake angle on the fault: The rake angle in case 3 is set to be -20°, which is left lateral strike-slip with including small normal fault slip, while that in case 1 and 2 is 0°. The simulated ground motions near the center of the fault trace in Case 3 showed large PGV for both FP and FN components.

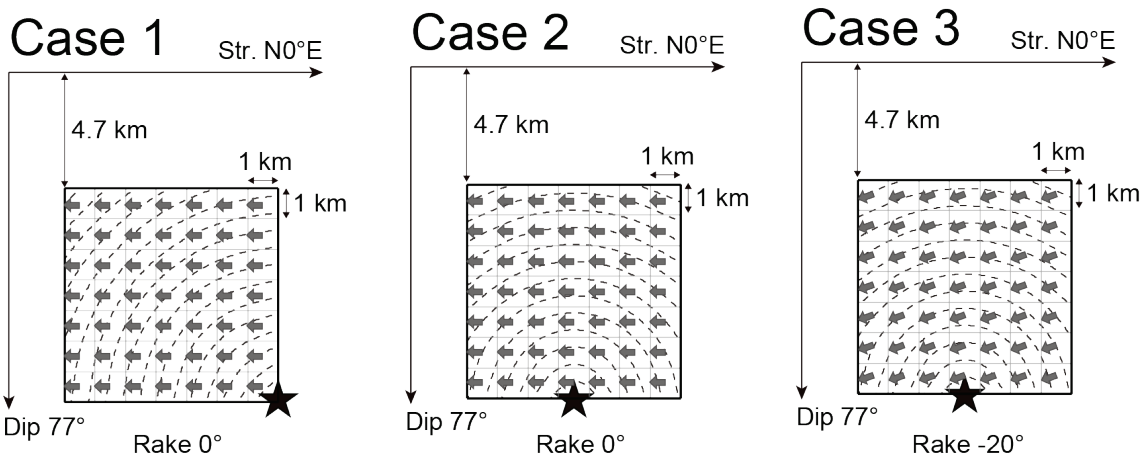

FIG. 10. Source models used in strong ground motion simulations in 0.1-3.0 Hz. The contour interval of rupture time is 0.2 s. The star indicates the rupture starting point. The gray arrows show slip directions of the hanging wall relative to the footwall.

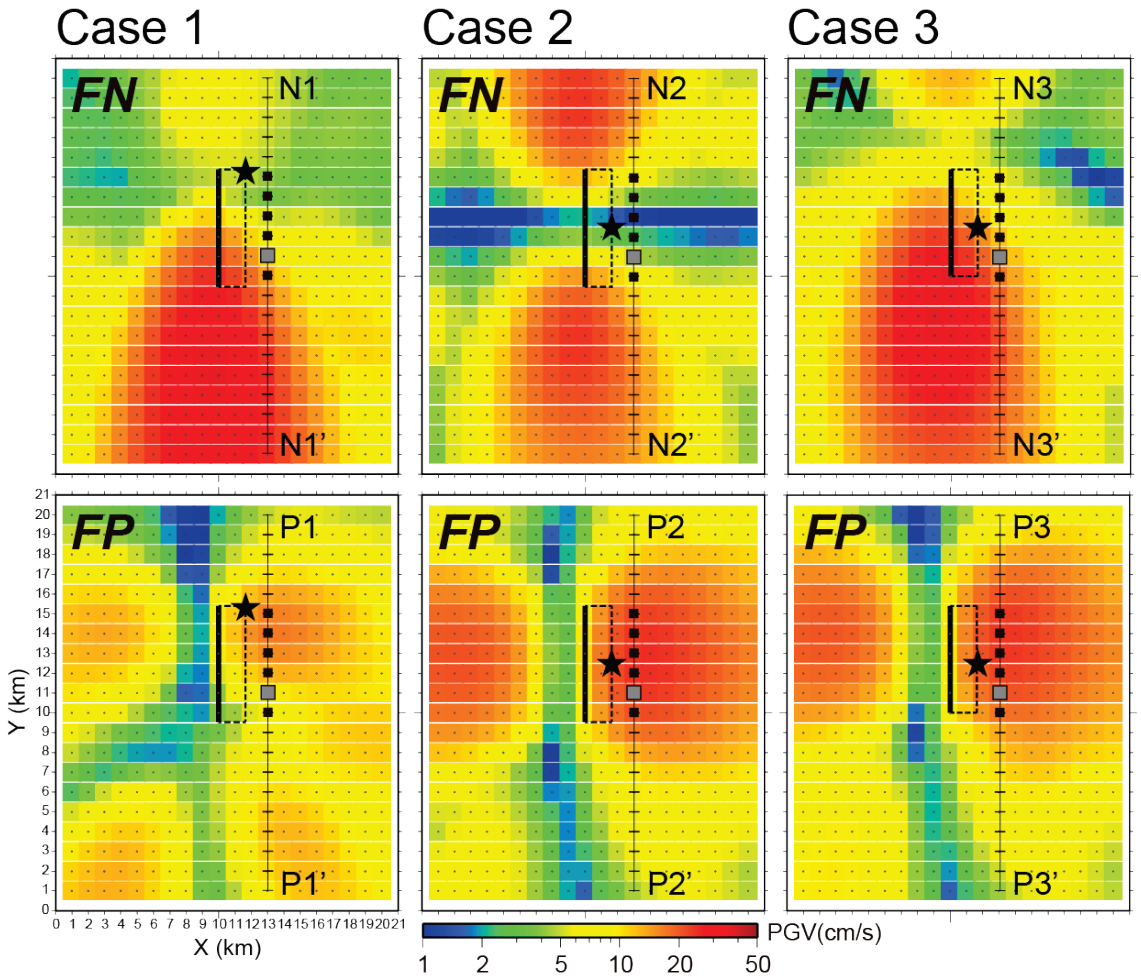

FIG. 11. Peak ground velocities on the ground surface predicted in the strong ground motion simulations for case 1 (left), 2 (middle), and 3 (right). Upper panels: Fault-normal component. Lower panels: Fault-parallel component.

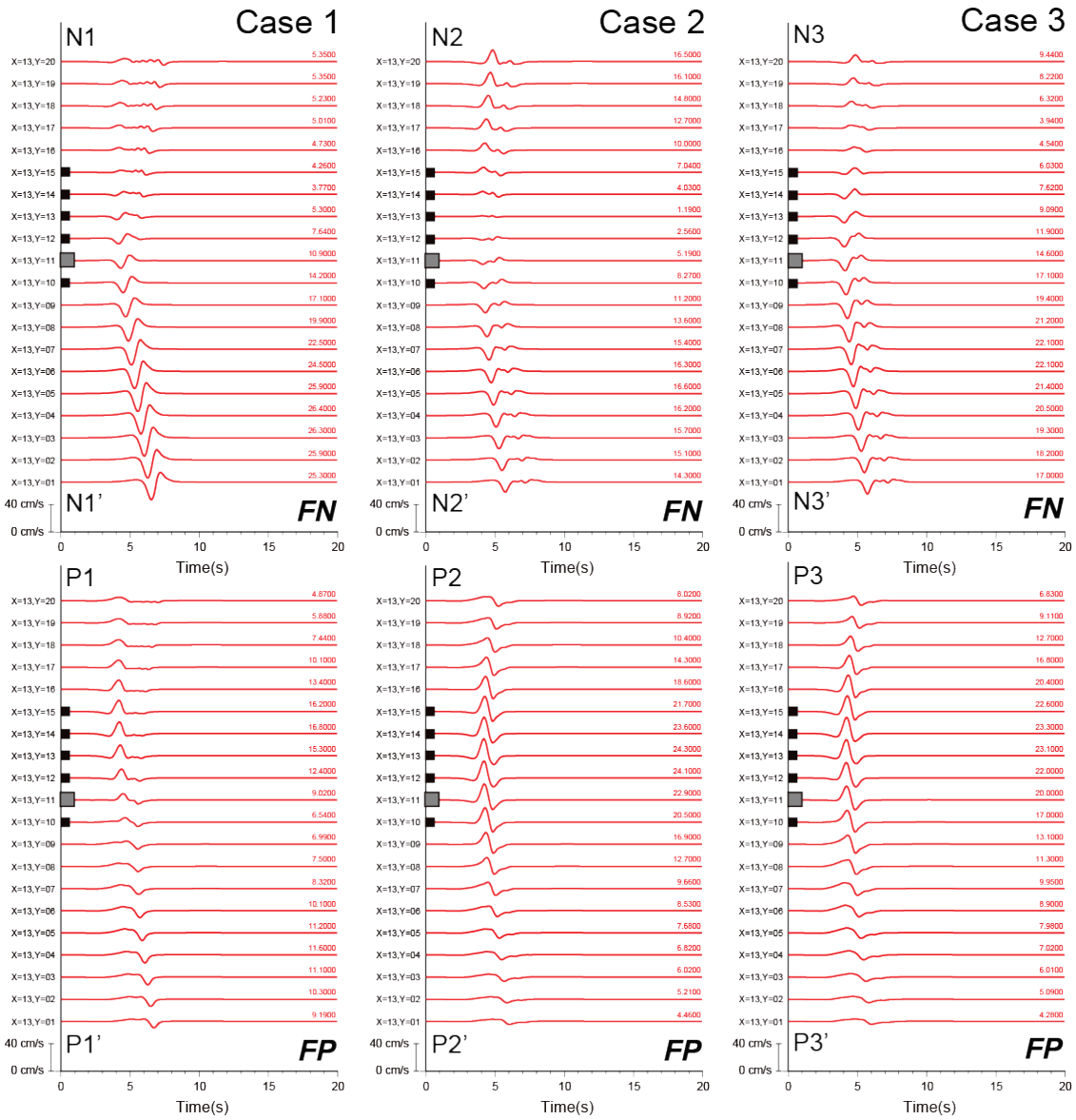

FIG. 12. Simulated velocity waveforms in 0.1-3.0 Hz. Solid squares on waveform traces indicate the site points shown in FIG. 11. The maximum amplitude of the observed waveform is shown above each trace in cm/s. The gray solid square point is an assumed station of KMMH16.

Figure 13 shows the synthetic waveforms at assumed station of KMMH16 comparing with the observed waveforms at 'real' KMMH16 station. The synthetic waveforms in Case 3 are better agreement with the observed waveforms at KMMH16 for both FP and FN components than those synthetics in Case 1 and 2. These results from ground motion simulations could suggest the strong pulses in FP and FN components at KMMH16 during *M*7.3 event was caused by the upward rupture directivity effect from the strike-slip fault with small normal-slip. We have to also note that the geometry of fault (strike and dip) near KMMH16 could be one of the key parameters to discuss the difference of ground motion between in FP and FN components. However, the oblique slip direction assumed in Case 3 is not way out of the heterogeneous slip distributions of kinematic source models (e.g., Asano and Iwata, 2016[3], Yoshida et al., 2016[4]) near SMGA2.

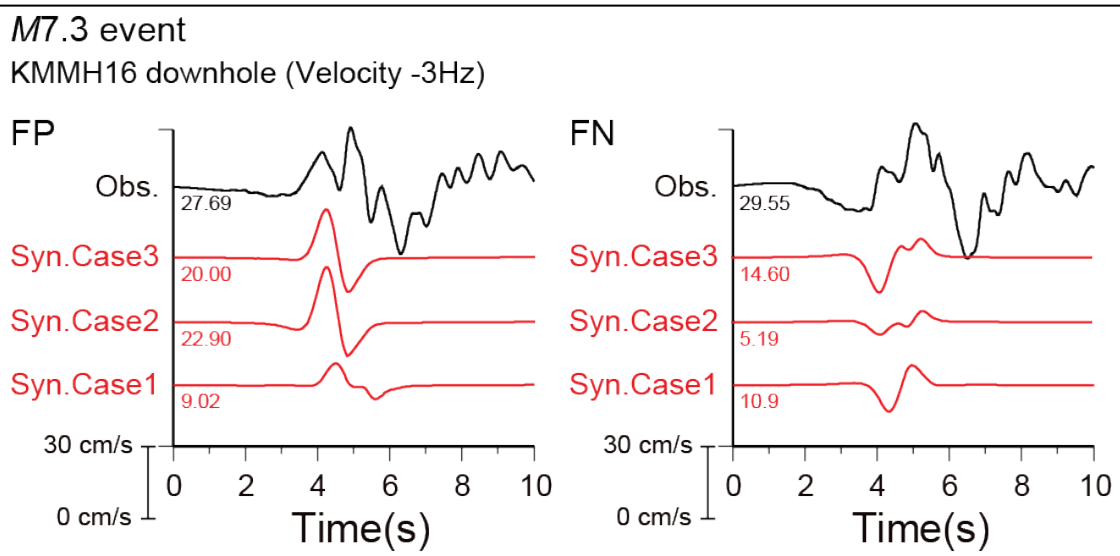

FIG. 13. Comparisons of velocity waveforms in FP (left) and FN (right) components at KMMH16 during M7.3 event between observation (black) and synthetic velocity waveforms (red) in 0.1-3.0 Hz on scenario Case 1, 2, and 3. The maximum amplitude of the waveforms is shown below each trace in cm/s.

5. Conclusions

We carried out the strong ground motion simulations based on the Strong Motion Generation Area (SMGA) source models for two large *M*6.5 and *M*7.3 events in the 2016 Kumamoto earthquakes. Strong ground motion simulations were performed in a broadband frequency range between 0.2 and 10 Hz by using the empirical Green's function (EGF) method. For *M*6.5 event, two squared SMGAs located near the large slip areas of kinematic inversion source model were estimated by the forward modeling through ground motion simulations. For *M*7.3 event, three-SMGA model on multi-segment fault model constructed by Irikura et al., (2017)[18] was used for ground motion simulations in this paper. These SMGA models for both *M*6.5 and *M*7.3 events were able to reproduce well the characteristics of observed ground motions in and around source areas, including the strong pulses observed at near-source station KMMH16. From the ground motion simulations based on both SMGA models and hypothetical simple source models, we concluded that the mechanisms of generating the strong pulses at KMMH16 during *M*6.5 and *M*7.3 events are following: The forward rupture directivity from two SMGAs with strike-slip caused the two distinct strong pulses in fault normal component during *M*6.5 event. Whereas, the upward rupture directivity along the fault dip direction from the SMGA with strike-slip including small normal-slip, which is located just beneath KMMH16, caused the strong pulse in both fault parallel and normal components during *M*7.3 event. These rupture directivity effects are quite important to estimate and predict the near-source strong ground motions for inland crustal earthquakes.

ACKNOWLEDGEMENTS

Strong motion data from K-NET, KiK-net and F-net were provided by the National Research Institute for Earth Science and Disaster Resilience (NIED), Japan. We also used moment tensor solutions routinely determined by F-net, NIED. The JMA unified earthquake catalog was produced by JMA in cooperation with the Ministry of Education, Culture, Sports, Science and Technology (MEXT). Most of figures are drawn by using the Generic Mapping Tools

(Wessel and Smith, 1998[27]). This study was based on the 2016 research project 'Examination for uncertainty of strong ground motion prediction for inland crustal earthquakes' by the Nuclear Regulation Authority (NRA), Japan.

REFERENCES

[1] NAKATA, T., and IMAIZUMI, T. (Ed.), Digital active fault map of Japan (2002), University of Tokyo Press, Tokyo.

[2] FUKUYAMA, E., et al., "Automated seismic moment tensor determination using on-line broadband seismic waveforms", Zisin 2 (J. Seismol. Soc. Jpn.) 51(1998), 149–156 (in Japanese with English abstract).

[3] ASANO, K., and IWATA, T., "Source rupture processes of the foreshock and mainshock in the 2016 Kumamoto earthquake sequence estimated from the kinematic waveform inversion of strong motion data", Earth Planets Space, 68:147(2016), DOI 10.1186/s40623-016-0519-9.

[4] YOSHIDA, K., et al., "Source process of the 2016 Kumamoto earthquake (Mj7.3) inferred from kinematic inversion of strong-motion records", Earth Planets Space, 69:64(2017), DOI 10.1186/s40623-017-0649-8.

[5] KATO, A., et al., "Foreshock migration preceding the 2016 M_w 7.0 Kumamoto earthquake, Japan", Geophys. Res. Lett., 43(2016), 8945–8953.

[6] UCHIDE, T., et al., "The 2016 Kumamoto–Oita earthquake sequence: aftershock seismicity gap and dynamic triggering in volcanic areas", Earth Planets Space, 68:180(2016), DOI 10.1186/s40623-016-0556-4.

[7] SUGITO, N., et al., "Surface fault ruptures associated with the 14 April foreshock (Mj 6.5) of the 2016 Kumamoto earthquake sequence, southwest Japan", Earth Planets Space, 68:170(2016), DOI 10.1186/s40623-016-0547-5.

[8] SHIRAHAMA, Y., et al., "Characteristics of the surface ruptures associated with the 2016 Kumamoto earthquake sequence, central Kyushu, Japan", Earth Planets Space, 68:191(2016), DOI 10.1186/s40623-016-0559-1.

[9] OZAWA, T., et al., "Crustal deformation associated with the 2016 Kumamoto Earthquake and its effect on the magma system of Aso volcano", Earth Planets Space, 68:186(2016), DOI 10.1186/s40623-016-0563-5.

[10] FUJIWARA, S., et al., "Small-displacement linear surface ruptures of the 2016 Kumamoto earthquake sequence detected by ALOS-2 SAR interferometry", Earth Planets Space, 68:160(2016), DOI 10.1186/s40623-016-0534-x.

[11] FDMA (FIRE AND DISASTER MANAGEMENT AGENCY), "The 2016 Kumamoto earthquake (111th report)", http://www.fdma.go.jp/bn/2016/detail/960.html. Accessed 20 Feb. 2018 (in Japanese).

[12] AOI, S., et al., "Deployment of new strong motion seismographs of K-NET and KiK-net", Earthquake data in engineering seismology. Geotechnical, geological, and earthquake engineering, Vol. 14 (Akkar S., et al., Ed), Springer, Dordrecht, 167–186.

[13] SUZUKI, W., et al., "Strong motions observed by K-NET and KiK-net during the 2016 Kumamoto earthquake sequence", Earth Planets Space, 69:19(2016), DOI 10.1186/s40623-017-0604-8.

[14] YAGI, Y., et al., "Rupture process of the 2016 Kumamoto earthquake in relation to the thermal structure around Aso volcano", Earth Planets Space, 68:118(2016), DOI 10. 1186/s40623-016-0492-3.

[15] KUBO, H., et al., "Source rupture processes of the 2016 Kumamoto, Japan, earthquakes estimated from strong-motion waveforms", Earth Planets Space, 68:161(2016), DOI 10.1186/s40623-016-0536-8.

[16] HAO, J., et al., "Slip history of the 2016 Mw 7.0 Kumamoto earthquake: Intraplate rupture in complex tectonic environment", Geophys. Res. Lett., 44(2016), 743–750.

[17] KOBAYASHI, J., et al., "Rupture processes of the 2016 Kumamoto earthquake sequence: Causes for extreme ground motions", Geophys. Res. Lett., 44(2016), 6002–6010.

[18] IRIKURA, H., et al., "Applicability of source scaling relations for crustal earthquakes to estimation of the ground motions of the 2016 Kumamoto earthquake", Earth Planets Space, 69:10(2016), DOI 10.1186/s40623-016-0586-y.

[19] MIYAKE, H., et al., "Source characterization for broadband ground-motion simulation: Kinematic heterogeneous source model and strong motion generation area", Bull. Seism. Soc. Am., 93(2003), 2531-2545.

[20] IRIKURA, K., "Prediction of strong acceleration motions using empirical Green's function", Proc. 7th Japan Earthq. Eng. Symp., Tokyo(1986), 151-156.

[21] SATOH, T., "Source, path and site effects of the 2016 Kumamoto earthquake, the foreshocks and aftershocks using the spectral inversion method", Abstracts of Japan Geoscience Union Meeting, (2016), MIS34-P71.

[22] FUJIWARA, H., et al., "A Study on subsurface structure model for deep sedimentary layers of Japan for strong-motion evaluation", Technical Note of the National Research Institute for Earth Science and Disaster Prevention, 337(2009).

[23] FUJIWARA, H., et al., "Some improvements of seismic hazard assessment based on the 2011 Tohoku earthquake", Technical Note of the National Research Institute for Earth Science and Disaster Prevention, 379(2012).

[24] KAMAE, K., and IRIKURA, K., "Source Model of the 1995 Hyogo-ken Nanbu Earthquake and Simulation of Near-Source Ground Motion", Bull. Seism. Soc. Am., 88(1998), 400-412.

[25] BOUCHON, M., "A simple method to calculate Green's functions for elastic layered media", Bull. Seism. Soc. Am., 71(1981), 959–971.

[26] KENNETT , B.L.N., and KERRY, N.J., "Seismic waves in a stratified half space", Geophys. J. R. Astr. Soc., 57(1979), 557–583.

[27] WESSEL, P., and SMITH, W.H.F., "New, improved version of Generic Mapping Tools released", Eos Trans., AGU, 79(1998), 579.